The Determination of Particle Size Distributions by Hydrodynamic Chromatography. An Analysis of Dispersion and Methods for Improved Signal Resolution

C. A. SILEBI and A. J. McHUGH, *Department of Chemical Engineering and Emulsion Polymers Institute, Lehigh University, Bethlehem, Pennsylvania 18015*

Synopsis

Various methods are described and compared for the determination of particle size distributions (PSD) in the submicron range by a technique known as hydrodynamic chromatography (HDC). Data are presented for a series of monodisperse latexes to establish the validity of the Mie theory of light scattering in describing the detector optical density signal. Analyses for the PSD involve corrections to the experimental HDC chromatograms for the effects of dispersion and are broadly classified as integral and numerical methods. Comparisons of calculations are made to chromatograms for polydisperse latexes as well as synthetic, discontinuous distributions and show the critical role of the optical density–particle size relationship in determining resolution and calculation stability. An integral method involving a non-Gaussian form for the dispersion function and a polynomial expansion for the chromatogram and an iterative numerical method involving modifications of a previously published technique are shown to give the best results for the PSD. The discussion includes an analysis of the possibility of improved signal resolution using turbidity in the absorption wavelength region and refractive index measurements. The conclusion is reached that increased resolution with turbidity is preferable to refractive index measurement since lower particle concentrations can be used.

INTRODUCTION

Hydrodynamic chromatography (HDC) is a technique for fractionating colloidal particles according to size, which was first developed by Small[1] and offers great promise as an efficient means for determining particle size distributions in the submicron range. In recent publications[2–4] calculations and results for further experimentation have been presented in terms of a mechanism for particle separation. Calculations were based on a model for the convected motion of Brownian particles through an equivalent array of capillary tubes which includes electrostatic force field effects. The analysis accounts explicitly for all the relevant experimental parameters, and the good agreement between calculated and measured separation factors means that the model can be used to study further effects, such as the determination of conditions for universal calibration and the possibility of separating equisized particles of differing chemistry.[3–5]

The ultimate impact of HDC as both an analytic method and a tool for experimental studies will rely heavily on the ease and accuracy with which the output chromatograms can be converted to particle size and particle size distribution.

The conversion of the HDC output signal can be achieved by either a funda-

Journal of Applied Polymer Science, Vol. 23, 1699–1721 (1979)
© 1979 John Wiley & Sons, Inc.
0021-8995/79/0023-1699$01.00

mental model for ‹ dispersion or, from a more practical viewpoint, using empirical methods ıe chromatogram, such as is done in GPC.[6] An attempt was made at the former approach[8] using an analysis based on a simplified Taylor dispersion model for peak spreading.[7] However, the results were only of marginal success. A principal shortcoming of the Taylor analysis in the present context is that it does not account properly for either the hydrodynamic wall effect[9] or the electrostatic forces, both of which lead to non-Gaussian, monodisperse peak spreading. Resolution in HDC is such that within a 3-ml volume, particles ranging from 90 nm to 360 nm in diameter will elute.[1,2]

The present analysis will show that this feature, combined with the non-Gaussian peak spreading which also occurs, has a profound effect on the signal conversion calculations. Thus, any fundamental analysis needs to account for the causes of non-Gaussian dispersion. The Brenner and Gaydos analysis[9] included dispersion effects and might in principle be extended to account for HDC peak spreading; however, the tractability of the calculations would seem doubtful. It may also be that, though the capillary tube model affords an excellent explanation for the single particle residence time behavior, it may be an inadequate means for predicting the effects of interstitial flow geometry on dispersion. For these reasons, the analyses presented in this paper have centered on methods for solving the integral dispersion equation. The discussion will show a comparison of various techniques which have been applied for calculating size distributions directly from the HDC chromatogram and will include calculations to show the important effect which the form of the output signal function has on particle size resolution.

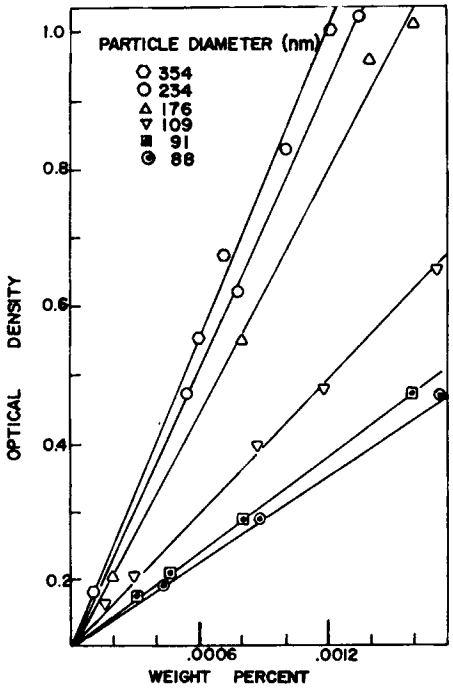

Fig. 1. Optical density vs particle weight percent for polystyrene standards at the 254-nm wavelength HDC operating conditions.

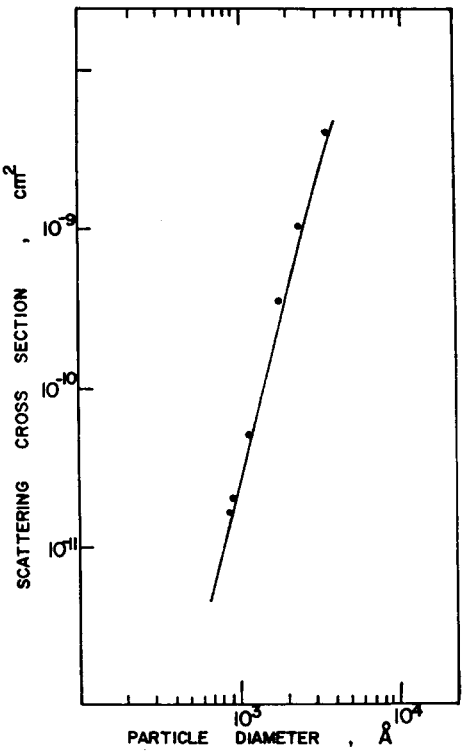

Fig. 2. Comparison between experimental and calculated scattering cross section for polystyrene standards.

All of the discussion involves data obtained with our current HDC setup on several monodisperse polystyrene standards (which have been discussed elsewhere[8]) and two polydisperse latexes: a neoprene latex supplied by du Pont and described elsewhere[5] and a polystyrene latex synthesized and characterized in our laboratories. Results of comparisons between calculated and measured size distributions will be presented for the polystyrene system, to be referred to as PS1 in the text. Similar results were found in all cases for the neoprene latex and can be found elsewhere.[5] The hydrodynamic chromatography unit consists of three columns packed with nonporous, spherical beads of a styrene–divinyl benzene copolymer. The output signal is optical density of the particle suspension, measured in a flow-through cell at 254 nm. Complete descriptions of the instrument and methods can be found in previous publications.[2,8] We begin the discussion with an analysis of the applicability of Mie light scattering theory to our instrument and considerations involving the column material balance.

DETECTION OF COLLOIDAL PARTICLES

The general theory of light scattering for nonabsorbing particles developed by Mie[10] has been previously applied to the turbidity output signal to compute relative amounts of known bimodal latex mixtures.[8] However, it has been noted in earlier studies of light scattering[11] that the corona effect and lateral scattering can be important sources of photometer measurement error, leading to signals differing significantly from Mie theory predictions. In addition, some contro-

TABLE I
Experimental Recoveries of The Monodisperse Polystyrene Standards from the HDC Columns

Particle diameter, Å	% Recovered
880	100
910	100
1090	100
1760	100
2340	90
3570	25

versy exists concerning whether polystyrene particles absorb light at 254 nm.[12,13] These observations suggest the need for an experimental evaluation of the output signal behavior. A series of tests were made of the photometric detector with concentrations of the various polystyrene standards kept below 0.0015 cm^3 solids/cm^3 solution, a value suggested by the studies of Churchill and co-workers[14] to avoid multiple scattering.

For colloidal suspensions which fulfill the conditions of single scattering, the relationship between extincted and transmitted light intensity is given by the familiar Lambert-Beer law:

$$\tau = \ln\left(\frac{I_0}{I}\right) = NR_{ext}x \tag{1}$$

where τ is the extinction coefficient; I_0 and I are the incident and transmitted beam intensities, respectively; x is the optical path length; N is the number of scattering and/or absorbing colloidal spheres per cm^3; and R_{ext} is the extinction cross section. Figure 1 shows a plot of the optical density signal, log (I_0/I), at various solids concentrations for a series of monodisperse polystyrene latexes at the detector operating wavelength of 254 nm. The linearity of the optical density (τ = 2.303 O.D.) with particle concentration establishes the applicability

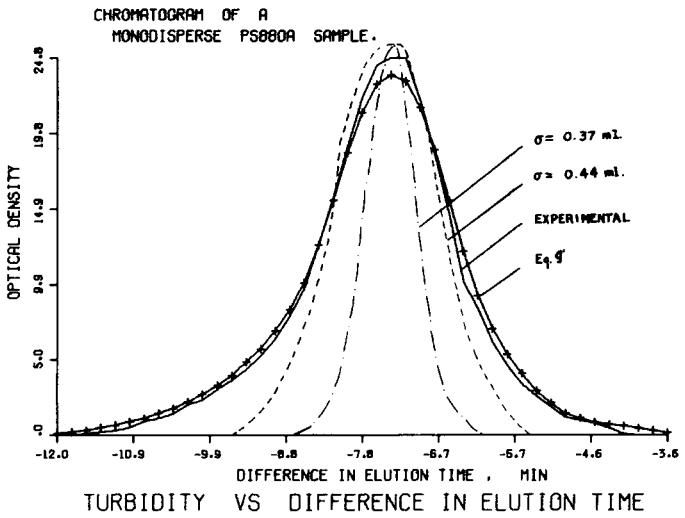

Fig. 3. Chromatogram of a monodisperse polystyrene sample compared to Gaussian functions with different σ values. Also shown is the curve generated from eq. (9′) of the text.

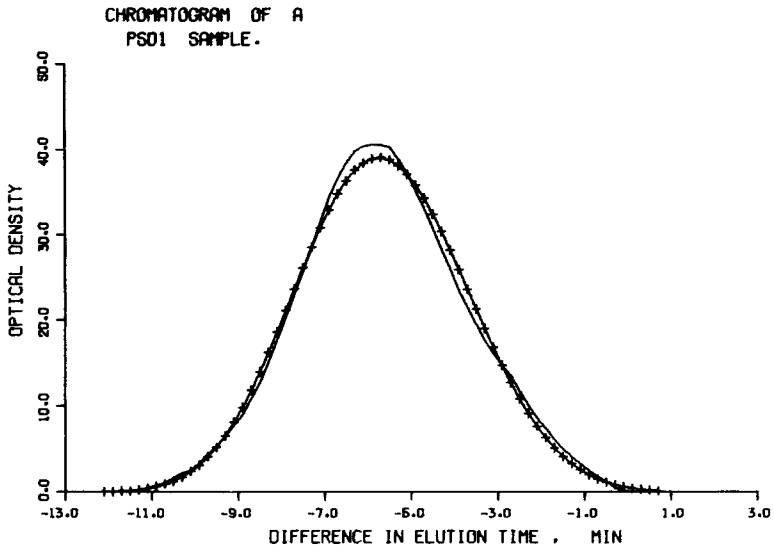

Fig. 4. Calculated (—) and experimental (+) chromatogram for the polydisperse polystyrene (PS1) sample. Computed chromatogram using five-parameter Hermite expansion.

of eq. (1) to these data. The slopes of Figure 1 can be used to calculate extinction cross sections from the limiting form of eq. (1) at low concentrations, which reads[15]

$$\left(\frac{\tau}{c}\right)_0 = 0.01 \left(\frac{\rho'}{\rho}\right) \frac{R_{\text{ext}}}{V_p} \tag{2}$$

where c is the weight fraction of colloid, ρ is the colloid density, and ρ' is the system density.

The calculations for the extinction cross section of spherical particles are developed in detail in several sources.[10,15,16] For nonabsorbing particles, the extinction cross section is equal to the scattering cross section, R_{scat}, and can be written[10]

$$R_{\text{scat}} = \frac{\lambda^2}{2\pi} \sum_{n=1}^{\infty} (2n + 1) (|a_n|^2 + |b_n|^2) \tag{3}$$

where λ is the wavelength of light in the medium; and a_n and b_n are functions of the refractive indices of the medium (m_2) and the particles (m_1) and of the ratio (R_p/λ_0) of the particle radius and the wavelength of light in vacuum. Figure 2 shows a comparison between scattering cross sections calculated from eq. (3) (solid line) and the experimental values (points) obtained with the aid of eq. (2). Values of m_1 were calculated from the Cauchy formula for the refractive index of polystyrene as a function of λ,[16] and m_2 was obtained from the International Critical Tables for water. The close agreement shown negates the possible instrument errors and indicates the applicability of Mie theory for calculating the photometer signal.

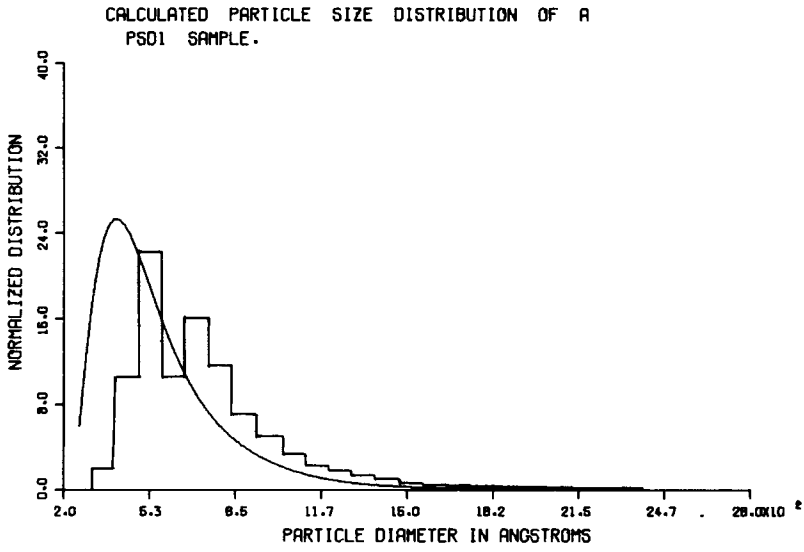

Fig. 5. Calculated PSD for PS1 sample of Fig. 4. Histogram represents PSD from electron microscopy.

RECOVERIES OF POLYSTYRENE STANDARDS

A material balance to determine the amount of injected sample eluting from the columns can be made from the resulting chromatogram when the volume and concentration of injected sample are known along with the particle size. Integration of eq. (1) over the entire elution volume for a monodisperse sample gives

$$N_T = \frac{1}{R_{ext}x} \int \tau \, dv \tag{4}$$

where N_T is the total number of particles eluting; and the integral represents the area under the chromatogram, W. The mass of exiting latex can thus be calculated after multiplication by the particle density and volume. Table I shows the recoveries obtained for different polystyrene sizes. It is seen that for particle diameters below 250 nm, recovery is complete; and, for the current setup, size distributions will only be valid for systems with particle sizes below about 300 nm.

AXIAL DISPERSION AND SIZE DISTRIBUTIONS

In order to correct an HDC chromatogram for axial dispersion by any mathematical technique, the relationship between the function $F(V)$, representing the experimental chromatogram, and the function $W(y)$, representing the area under the chromatogram due to the species with a mean retention volume y, must be first established. For a monodisperse system the chromatogram can be expressed as

$$F(V) = W\,G(V) \tag{5}$$

where $G(V)$ is the normalized instrumental spreading function for the particles. For a polydisperse system of n species, $F(V)$ will be given by a linear summation

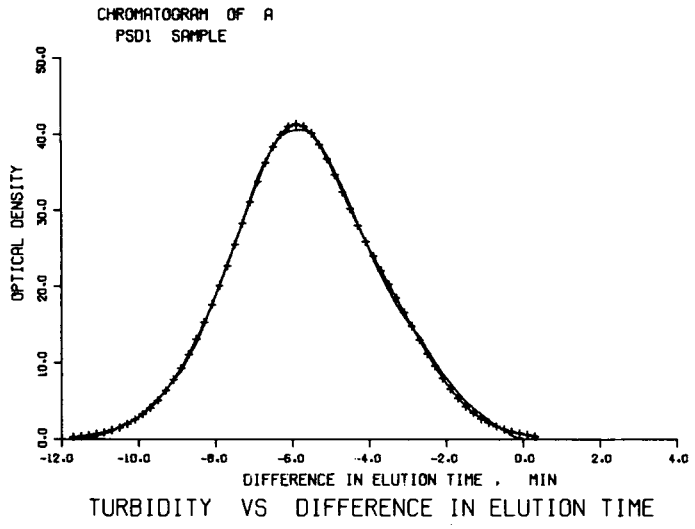

Fig. 6. Experimental (—) and calculated (+) chromatogram for the PS1 sample using the integral of the non-Gaussian kernel and five parameters in the distribution function.

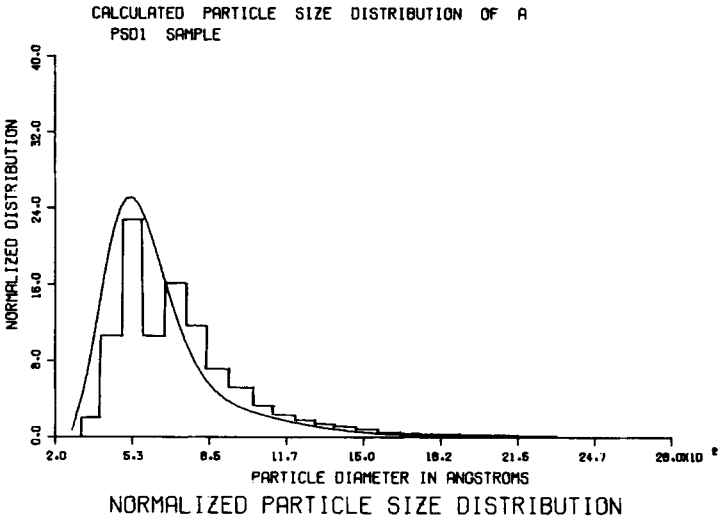

Fig. 7. Calculated PSD and measured histogram for PS1 of Fig. 6.

of the individual species contributions since, at the concentrations used (0.01% by weight), multiple scattering does not occur. Thus,

$$F(V) = \sum_{j=1}^{n} W_j G_j(V) \tag{6}$$

where W_j and $G_j(V)$ represent the area and normalized spreading function for species j. The area W_j is related to the number of j particles through eq. (4):

$$N_j = \frac{W_j}{xR_{\text{ext},j}} \tag{4'}$$

where $R_{\text{ext},j}$ is now the extinction cross section for species j. When the number of species is very large, W_j can be replaced by a continuous function $W(y)$ and eq. (6) becomes

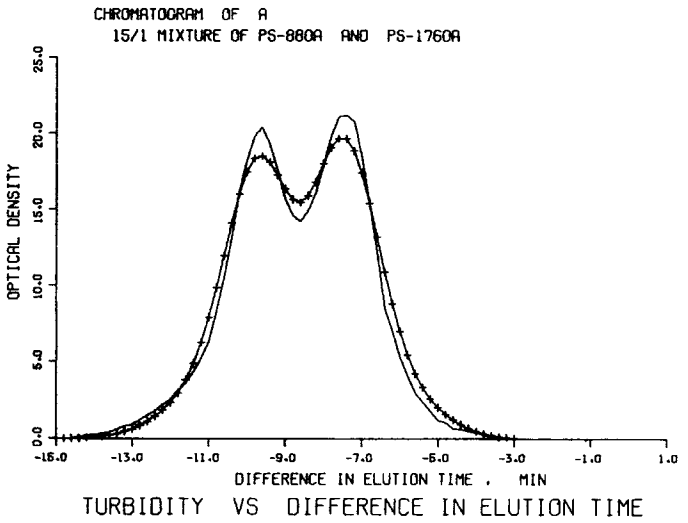

Fig. 8. Calculated (+) and theoretical (—) chromatogram of a 15:1 by number mixture of 88-nm and 176-nm standards using the approach in Fig. 6 and three parameters.

$$F(V) = \int W(y)\, G(V,y)\, dy \tag{6'}$$

where $G(V,y)$ is the normalized spreading function of the component with mean retention volume y, referred to as the kernel function. Equation (6') is the familiar axial dispersion equation developed for GPC and is often referred to as Tung's equation.[17] As indicated earlier, in the region of low ionic strength universal calibration behavior results, and the observed relationship between elution volume (or equivalently the difference in elution volume between marker and particle peaks) for polystyrene standards can be used.[2,3,18] For such conditions,

$$y = M_v \ln D_p + b \tag{7}$$

where M_v and b are calibration constants, and D_p is the particle diameter. The normalized differential particle size distribution $\phi(D_p)$ is related to $W(y)$ by

$$\phi(D_p) = \frac{\dfrac{d\Omega}{dD_p}}{\displaystyle\int \frac{d\Omega}{dD_p} dD_p} = \frac{\dfrac{d\Omega}{dy}\dfrac{dy}{dD_p}}{\displaystyle\int \frac{d\Omega}{dy}\frac{dy}{dD_p} dD_p} \tag{8}$$

where Ω is the cumulative or integral distribution function whose y derivative yields $W(y)$. Thus, substitution from eq. (7) gives the normalized distribution in terms of $W(y)$ as

$$\phi(D_p) = \frac{M_v W(y)}{D_p \displaystyle\int W(y)\, dy} \tag{8'}$$

The solution of eq. (6') for $W(y)$ involves two problems. First, it is necessary to represent the instrument spreading function by an approximate function and

to determine the numerical values for its parameters. The second problem involves the choice of an appropriate mathematical technique for solving the integral eq. (6′). A critical feature to be shown by the present analyses is the highly nonlinear conversion between $N(y)$ and $W(y)$ in eq. (4′). This necessitates accurate fitting of the chromatogram, especially in the small particle size region, and leads in most case to problems of ill-conditioning.

Methods selected for solving eq. (6′) or (6) followed variations of standard techniques developed for GPC analysis (e.g., see ref. 6 for a review) and can be broadly classed as integral or numerical.

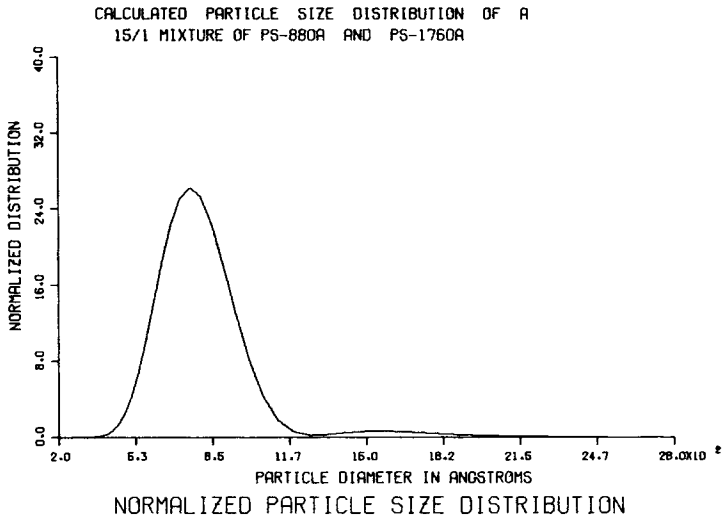

Fig. 9. Calculated PSD for synthetic mixture of Fig. 8. Area ratio is 35:1

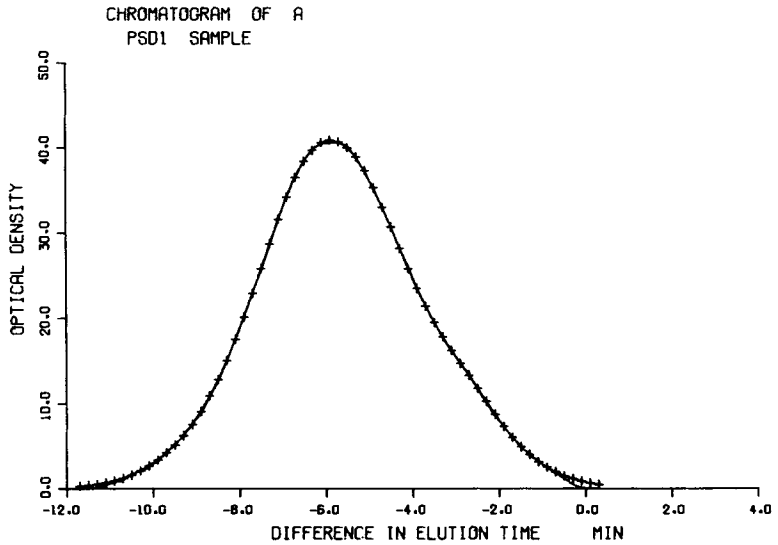

Fig. 10. Experimental (—) and calculated (+) PS1 chromatogram using the second iterative method of Ishige et al.[23]

INTEGRAL METHODS

As indicated, the first step in solving eq. (6′) involves fitting the kernel function $G(V,y)$. In the special case of Gaussian instrument spreading, the kernel function can be represented by

$$G(V,y) = \frac{1}{(2\pi\sigma)^{1/2}} \exp\left[-\frac{(V-y)^2}{2\sigma^2}\right] \tag{9}$$

where σ is the standard deviation of the distribution and is given by the square root of the second moment of the normalized chromatogram of the single species. In cases where eq. (9) holds, the natural method of solution of eq. (6′) involves an expansion of $F(V)$ in terms of the Hermite polynomials and polynomial expansion for $W(y)$.[17] The coefficients of the polynomial are determined by taking moments of the chromatogram and invoking the orthogonality condition.

Figure 3 shows a typical monodisperse chromatogram for the polystyrene standards compared to calculations from eq. (9) for two different σ values. It is clear that the single-species chromatogram is not adequately represented by eq. (9). Nonetheless, the method was applied using an average value of σ equal to 0.44 ml. Computation for the neoprene and polydisperse polystyrene samples showed improved fitting of the chromatogram with increased numbers of polynomial terms. However, an upper limit occurs beyond which increased terms lead to oscillations in the distribution function. The number of terms leading to the instability increases with increased polydispersity of the sample.

Figure 4 shows the fit to the chromatogram which occurs for a five-parameter Hermite expansion for the PS1 sample, and Figure 5 shows the resulting PSD calculation as compared to the histogram determined from electron microscopy. Similar results occurred for the neoprene sample, and in both cases small errors in the chromatogram fit in the small-particle region resulted in larger errors in the predicted number of small particles. This is a reflection of the small values for R_{ext} in eq. (4′) for the small particles.

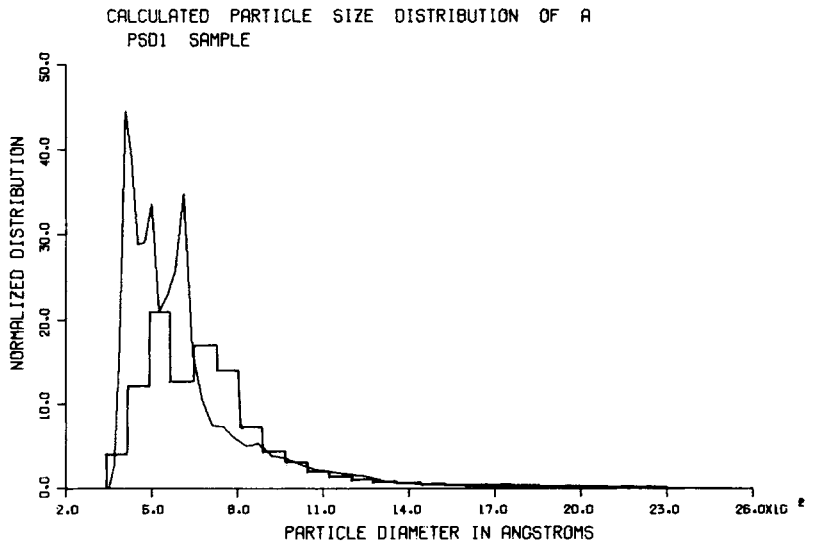

Fig. 11. Calculated PSD for PS1 from chromatogram of Fig. 12 compared to experimental histogram.

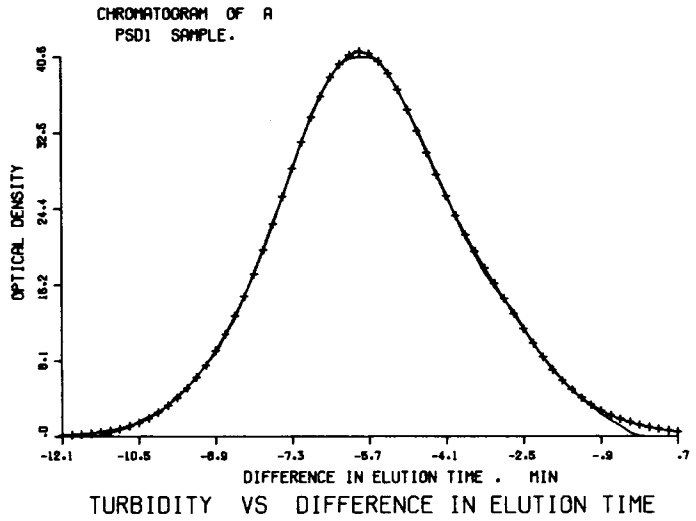

Fig. 12. Experimental (—) and calculated (+) PS1 chromatogram using modified method described in text.

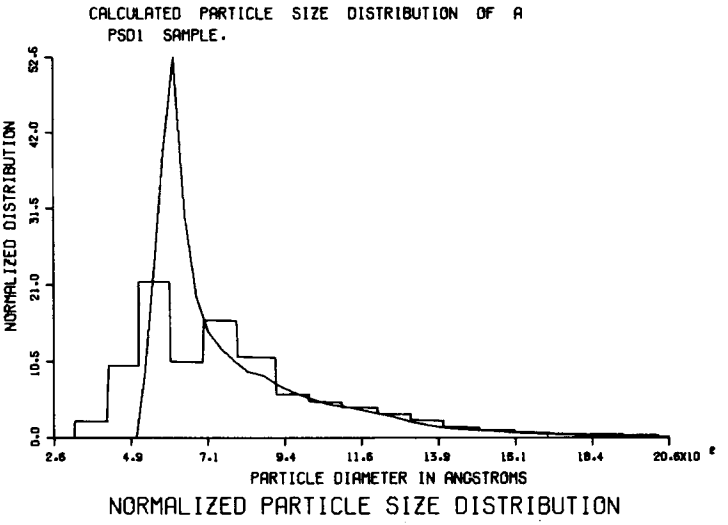

Fig. 13. Calculated PSD of Fig. 14 compared to experimental histogram.

Recently, Provder and Rosen[19] suggested a general statistical spreading function to account for skewed single-species chromatograms. The function coefficients describe symmetrical axial dispersion, skewing, and flattening of single-species chromatograms. However, the tailing at both ends of monodisperse HDC chromatograms is such that more than six coefficients would be needed. The HDC single-species chromatograms are nearly symmetrical; and, since the small particle region is the most important to fit, the following expression was used instead:

$$G(V-y) = \exp\left[-\frac{(V-y)^2}{2\sigma^2}\right] \sum_{m=0}^{n'} b_m \left(\frac{V-y}{\sigma}\right)^m \qquad (9')$$

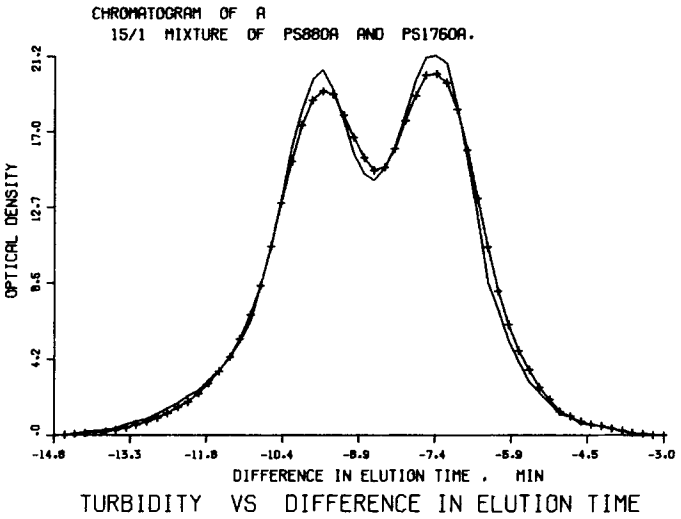

Fig. 14. Calculated (+) chromatogram for synthetic mixture 15:1 by number of 88-nm and 176-nm polystyrene standards, (−) synthetic chromatogram.

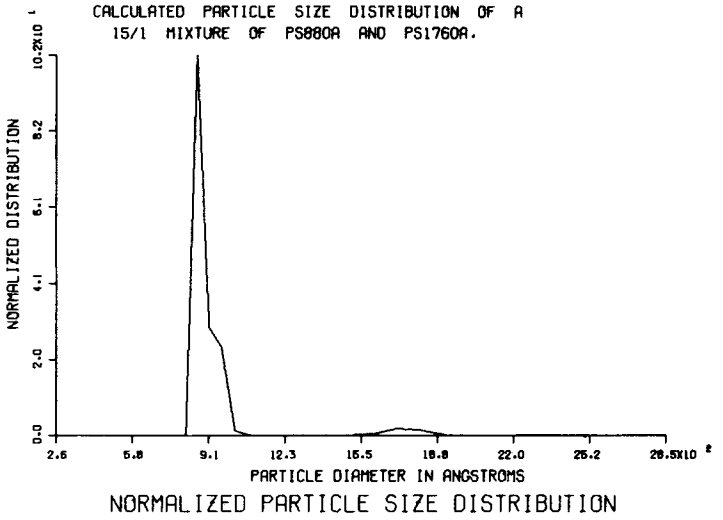

Fig. 15. Calculated PSD for Fig. 16. Area ratio is 20:1.

Substitution of eq. (9′) into eq. (6′) along with the polynomial expansion of $W(y)$ given by

$$W(y) = \exp\left[-p^2(y - y_0)^2\right] \sum_{i=0}^{n} R_i (y - y_0)^i \tag{10}$$

yields the following expression for $F(V)$:

$$F(V) = \exp\left[\frac{-p^2 y_0^2}{2l^2\sigma^2}\right] \left\{ \sum_{i=0}^{n} \left[\frac{R_i}{l^{i+1}} \sum_{k=0}^{i} {}_kC_i \left(\frac{y_0}{2l\sigma^2}\right)^k \right.\right.$$
$$\times \left((-1)^{i-k} \sum_{m=0}^{n'} \frac{b_m}{l^m} \sum_{j=0}^{m} {}_jC_m \left(\frac{p^2 y_0}{l}\right)^j \right.$$
$$\left.\left.\left. \times \left(\frac{1 + (-1)^{i-k+m-j}}{2}\right) \Gamma\left(\frac{i - k + m - j + 1}{2}\right) \right) \right] \right\} \tag{11}$$

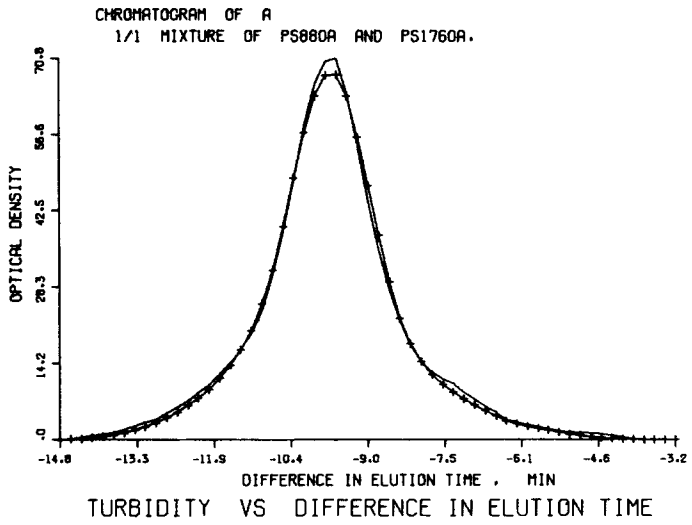

Fig. 16. Calculated (+) chromatogram for 1:1 synthetic mixture of 88-nm and 176-nm standards, (−) synthetic chromatogram.

where the ${}_eC_f$ are the binomial coefficients; $\Gamma(g)$ is the gamma function; p and y_0 are the reciprocals of the standard deviation and mean of the chromatogram, respectively; b_m is the coefficient defined by eq. (9′) to fit the chromatogram of a single species; and l is given by

$$l^2 = p^2 + \frac{1}{2\sigma^2} \tag{11′}$$

For eq. (9′) the coefficients used were b_0, b_4, b_8, and b_{16}, with values 1.0, 0.1, 1.2×10^{-2}, and 4.5×10^{-6}, respectively. Figure 3 shows the fit obtained for a 88 nm standard. The coefficients R_j, from which the distribution function $W(y)$ is obtained, were evaluated by minimizing the square of the error between the calculated and experimental chromatogram for the number of terms n that were

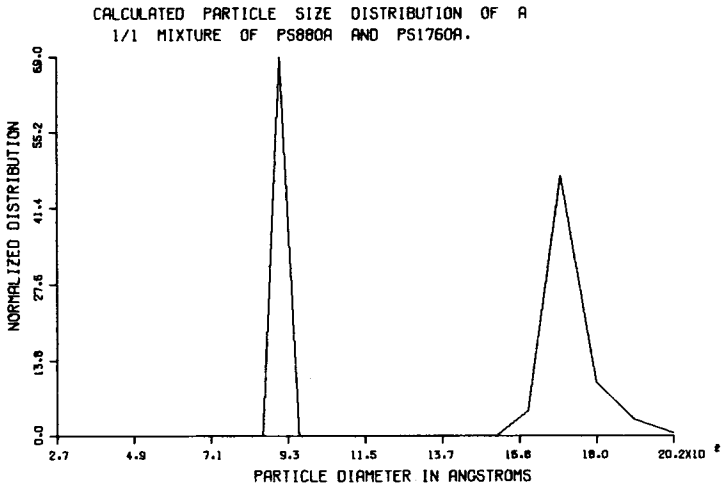

Fig. 17. Calculated PSD from Fig. 18. Area ratio is 1.5:1.

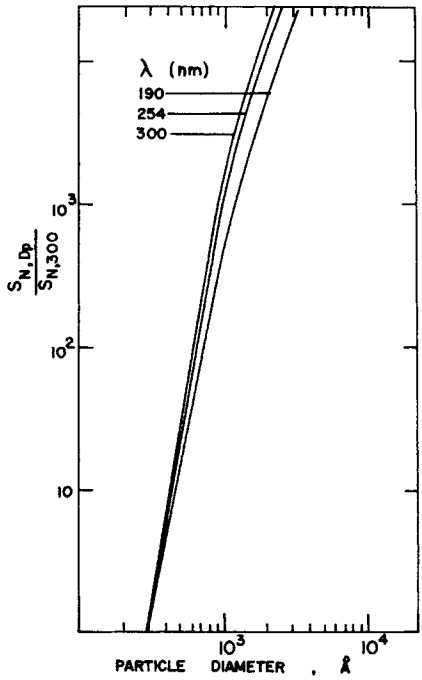

Fig. 18. Relative signal with respect to an equal number of nonabsorbing 30-nm particles at different wavelengths. Refractive index of medium and particles taken as 1.35 and 1.70, respectively.

used. As with the Hermite polynomials method, this technique leads to a maximum number of terms beyond which oscillations appear.

This approach was applied to the neoprene and PS1 samples as well as to a synthetic mixture comprised of two monodisperse sizes, 88 and 176 nm, in a 15:1 number ratio. Results for the PS1 and synthetic mixtures are shown in Figures 6 to 9. As can be seen, the method gives PSD values that compare favorably to the electron microscopy results for broad distributions, and the fit of the chromatogram is good. However, the bimodal distribution was not as closely predicted. Since the method is based on the assumption of a continuous distribution function, it is more appropriate for well-behaved polydisperse systems. For discontinuous distributions, it seems more appropriate to employ numerical methods since no analytic function is appropriate to represent such discontinuities.

NUMERICAL METHODS

The earlier numerical methods used for solving Tung's dispersion equation[17,19,20] did not lead to satisfactory results in all cases. For instance, for narrow distributions, oscillations result in the distributions which have been shown to be the result of the mathematical technique as well as detector noise. The method developed by Pickett et al.[21] for GPC has been applied to HDC analysis[22] in conjunction with a Gaussian spreading function and found to be unsuitable. In this section, two numerical techniques previously used in GPC analysis will be evaluated along with a proposed modification to the second method presented by Ishige et al.[23]

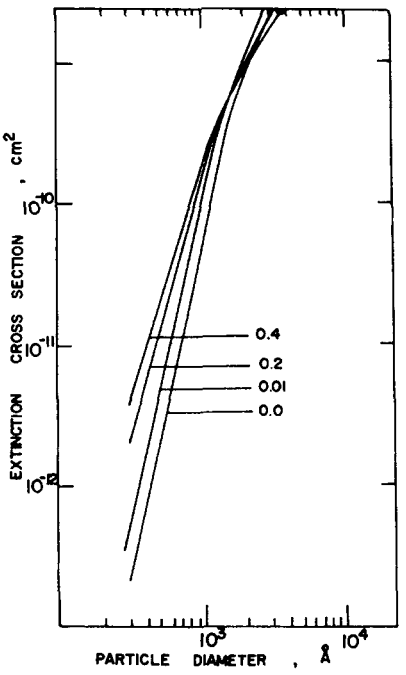

Fig. 19. Effect of imaginary part of the complex index of refraction on the particle extinction cross section at 200 nm wavelength. Real part of refractive index for the particles and medium taken as 1.70 and 1.35, respectively.

Stoisits[8,18] applied a least-squares method to calculate the relative amounts of mixtures of two monodisperse samples with results comparing favorably to the electron microscopy counts. However, the method assumed a prior knowledge of the particle sizes present in the mixture. An extension of this method to the neoprene and PS1 polydisperse systems was used. Simpson's rule was employed, assuming a number of sizes with equally spaced elution volumes, to evaluate the integral. The function $G_j(V)$ was again approximated by eq. (9′), and the following features were observed. When no restrictions to the W_j values

TABLE II
Mixture Rule for Index of Refraction[a]

Theoretical	
i. Newton	$n_{12}^2 = \phi_1 n_1^2 + \phi_2 n_2^2$
ii. Lorentz–Lorentz	$\frac{n_{12}-1}{n_{12}^2+2} = \frac{n_2^2-1}{n_2^2+2}\phi_2 + \frac{n_1^2-1}{n_1^2+2}\phi_1$
iii. Wiener	$\frac{n_{12}^2-n_2^2}{n_{12}^2+2n_2^2} = \frac{n_1^2-n_2^2}{n_1^2+2n_2^2}\phi_1$
Empirical	
i. Lichtenecker	$\log n_{12} = \phi_2 \log n_2 + \phi_1 \log n_1$
ii. Avogadro–Biot Beer–Landolt Christiansen– Wintgen	$n_{12} = \phi_1 n_1 + \phi_2 n_2$

[a] From reference 27; n_{12} = refractive index of dispersion; n_1 = refractive index of particle; n_2 = refractive index of medium; ϕ_1 = volume fraction of particles; ϕ_2 = volume fraction of medium.

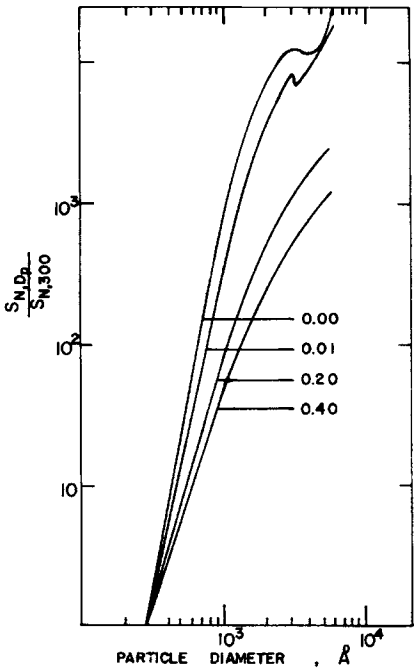

Fig. 20. Effect of imaginary part of the complex index of refraction on the relative number signal. Same parameters as Fig. 22.

were applied, negative numbers for the distribution resulted when the number of sizes assumed exceeded a critical value, depending on the degree of polydispersity. This result is reminiscent of the severe oscillations reported by other investigators.[17] Since only nonnegative W_j values are meaningful, an alternate approach was used by setting the minimum W_j to zero; however, the oscillation problem was not eliminated. The fit of the chromatogram using this approach was good, but the PSD values did not compare favorably.[5]

Two methods have been proposed by Ishige et al.[23] which involve calculating $F(V)$ from an initial guess of $W(y)$ and iteratively correcting $W(y)$ according to the comparison between calculated and experimental chromatograms at each iteration level. In the first method the correction is based on a difference, while for the second it is based on the ratio between the computed and experimental chromatogram. The first method can lead to oscillations at both ends of the distribution function, while the attractive feature of the second method is the elimination of the possibility of negative $W(y)$.[23] The latter results from the fact that any chromatogram $F(V)$ always has a broader distribution than the input $W(y)$. Hence, if the calculated chromatogram F^* is broader than F, the assumed $W_{j,i}$ must be sharpened to give a closer response to F. The corrected $W_{j,i}$ is given by $W_{j+1,i}$ and is calculated as follows[23]:

$$W_{j+1,i} = \left(\frac{F_i^*}{F_i}\right) W_{j,i} \tag{12}$$

where i refers to the elution volume considered and j is the level of iteration. Although negative $W_{j,i}$ values are impossible by this method, convergence is not guaranteed. The method was applied to the polydisperse samples, and since

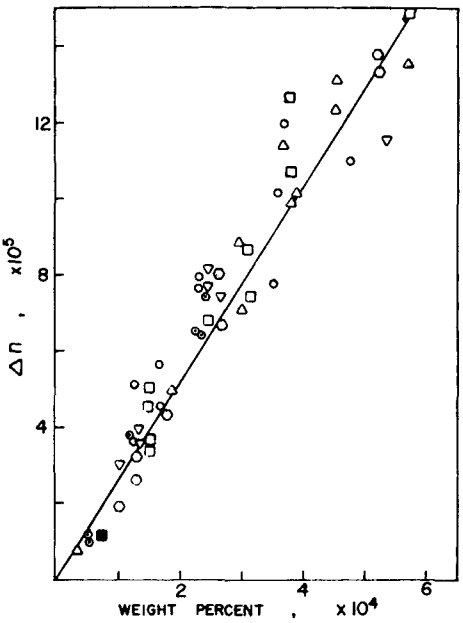

Fig. 21. Differential refractive index of polystyrene standards in water at different concentrations. (□) 88 nm; (△) 91 nm; (○) 109 nm; (▽) 176 nm; (○) 234 nm; (⊙) 357 nm.

it is completely numerical, data were used directly from the monodisperse chromatograms, eliminating the need for a specific spreading function to characterize them. Because of the limited number of monodisperse chromatograms, they were used to represent the spreading behavior for particle ranges as follows: For particles less than 90 nm, the 88-nm standard was used; in the range of 90 to 130 nm, the 109-nm standard was used; in the range of 130 to 200 nm, the 176-nm standard was used; and for sizes larger than 200 nm, the 234-nm standard was used.

Figures 10 and 11 illustrate results for the PS1 sample where a good fit of the chromatogram was accomplished; however, the PSD does not compare favorably. This was especially true in the small-particle region, which again corresponds to the region of high detector sensitivity. As indicated, this method has the advantages of using experimental monodisperse chromatograms and eliminating the oscillation problem. The principal shortcoming is the one-to-one correction used at each reading. This assumes that the contribution at each elution volume is due only to the particle eluting at the volume and is independent of the other particles. Inclusion of contributions due to neighboring sizes is possible by a geometric averaging of each species correction.[5] The weighting exponents are taken from the relative contributions of the sizes within $\pm 2\sigma$ of the elution volume considered and then normalized to unity for the sum of the exponents. The correction to $W_{j,i}$ is thus written as

$$W_{j+1,i} = \prod_{k=-n'}^{k=n'} \left(\frac{F^*_{i+k}}{F_{i+k}} \right)^{\gamma_{i,k}} \tag{12'}$$

where the exponent $\gamma_{i,k}$ is given by

$$\gamma_{i,k} = \frac{\gamma_{i+k}}{\Sigma \gamma_{i+k}} \tag{13}$$

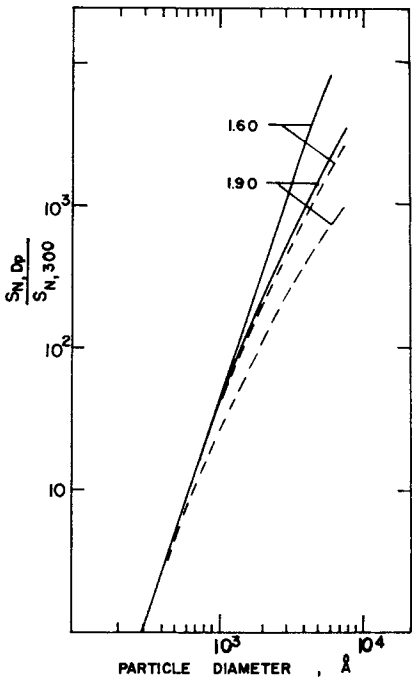

Fig. 22. Effect of refractive index of particles on the number relative signal at two wavelengths: (—) 500 nm; (- - -) 300 nm. Medium refractive index is 1.35.

and in eq. (12′) the symbol Π stands for the continued product. The number of symmetrical terms n' about F_i was chosen according to the single-species spread to include points located within $\pm 2\sigma$ of the elution volume of interest. Figures 12 and 13 illustrate the chromatogram fit and PSD achieved for the PS1 sample by this method. The fit is seen to be reasonably good for the larger particles. Similar results were obtained for the neoprene latex. Again it must be emphasized that a small mismatch in the small-particle range results in an appreciable error for the PSD for that region.

Figures 14 and 15 are respectively the chromatogram and PSD obtained for the 15-to-1 synthetic mixture of the monodisperse 88-nm and 176-nm standards. In this case detection of peak resolution has been achieved and the calculated ratio given by the areas under the chromatogram is now 20:1. Figure 16 shows the chromatogram for a 1-to-1 by number mixture of 88-nm and 176-nm standards where, as a result of the signal detector characteristics, the smaller-particle population shows only as a small shoulder in the output despite the fact that the smaller particles represent 50% of the total particle numbers. Figure 17 illustrates that the iterative method predicts the presence of the two populations although the number ratio of 176-nm to 88-nm particles has changed to 1.5:1.

METHODS FOR IMPROVED SIGNAL RESOLUTION

The calculations for particle size distribution demonstrate the critical role of eq. (4′) in controlling both instrument resolution and dispersion calculation sensitivity. The results presented point to the need for improved signal characteristics as well as possible improvements in column dispersion through

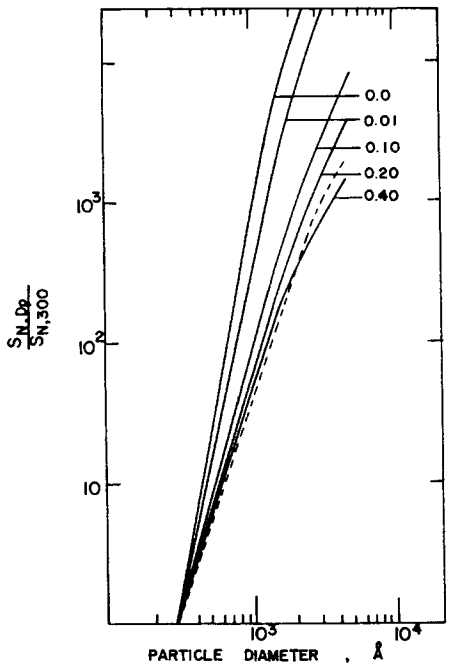

Fig. 23. Comparison between number relative signals for differential refractometric and photometric detection. Real refractive indices of particle and medium are 1.70 and 1.35. Wavelengths are 200 nm for photometer and 500 nm for refractometer.

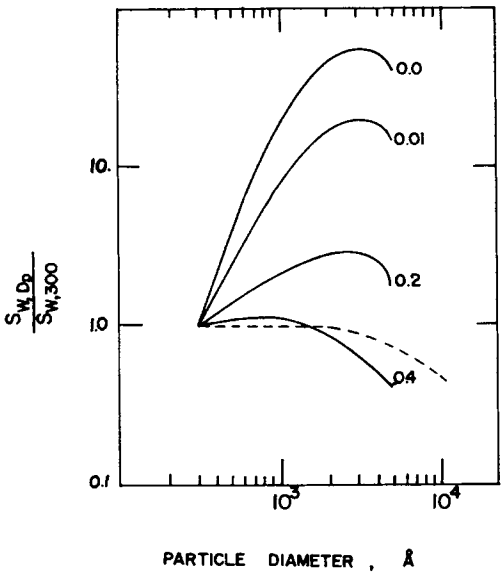

Fig. 24. Comparison for weight relative signals from differential refractometry and photometric detection. Parameters same as in Fig. 23.

modified flow geometry and packing characteristics. In this section we shall discuss calculations which have been addressed to the improvement of signal resolution. A later publication will be addressed to experiments currently in progress concerning the latter of the above approaches.

Improvements in the detection system have been suggested previously, such as use of a photometer with a shorter wavelength[8] to detect relatively small particles. Also, as in GPC, the use of differential refractometry has been shown to produce a better signal than the one obtained with a 254-nm photometer.[24] A detailed analysis of such potential improvements is necessary in order to determine the advantages either of the suggested methods may offer. Since at wavelengths less than 254 nm, polystyrene is likely to be an absorbing species, the theoretical evaluation of such a detecting device must account for this. Consider first the improvement possible with shorter wavelength turbidity.

IMPROVEMENTS IN THE TURBIDITY SIGNAL

A series of calculations were made to determine the effects of parameter variations on the optical density signal intensity as predicted by Mie theory. The parameters studied were wavelength of the incident beam, real refractive index and imaginary refractive index of the particles, and particle size. Optical density was calculated from eq. (1) where now, to account for absorption, the more general expression for R_{ext} was used, where[10]

$$R_{ext} = \frac{\lambda^2}{2\pi} \sum_{n=1}^{\infty} (2n + 1) Re(a_n + b_n) \tag{14}$$

The coefficients a_n and b_n in eq. (14) are given elsewhere[10] in terms of the Bessel and Neumann functions. When the argument is complex, as it is for absorbing spheres, the computation of a_n and b_n is more conveniently accomplished by the method proposed by Aden.[25]

Calculations for the effects of source wavelength and variations in the refractive index for nonabsorbing spheres are illustrated elsewhere.[5] The results showed that a decrease in wavelength and/or increasing the refractive index in general increases the scattering cross section, though a combination of small wavelength and large index of refraction shows a reversal for large particle sizes. From this result we conclude that by using shorter wavelengths, the absolute signal for small particles will be increased. However, for obtaining particle size distributions, the relative signal is of greater importance.

Figure 18 is a plot of the ratio of the signal S, obtained for N particles of diameter D_p, to the signal resulting from N particles of diameter 30 nm as a function of particle diameter for various wavelengths for nonabsorbing particles. The change of wavelength can be seen to have a small influence on the relative signal. Similar calculations for various refractive indices showed essentially no change in relative signal at 254 nm. The calculations were made for nonabsorbing particles; however, some polymeric materials have shown appreciable absorbance at certain wavelengths in the UV region, including polystyrene.[26] This possible effect can be accounted for in terms of the imaginary part of the refractive index. Calculations of the extinction cross section for different values of the imaginary part of the refractive index, which includes the range from weak to strong light absorbers, are shown in Figure 19. These calculations illustrate that the extinction cross section of the smaller particles is greatly enhanced while that of the larger ones slightly decreases. The first feature suggests better detection of the smaller particles, while the second feature suggests an improvement of the relative signal. Figure 20 is an illustration of this very last fact which we

believe is of transcendental importance for the determination of PSD in HDC.

DIFFERENTIAL REFRACTOMETRY DETECTION

Latexes with a refractive index different from the medium can be detected by monitoring the change of refractive index of the exiting system. The relationship between the difference in refractive index and the concentration of the dispersion has been treated theoretically and empirically by several investigators. The various mixture rules shown in Table II are, however, all limited to the case where the relative diameter α ($\alpha = \pi D_p/\lambda$) is small and the refractive index ratio is near unity.[27] Such restrictions, similar to the ones of Rayleigh scattering, limit the applications to a small fraction of the colloidal range. Zimm and Dandliker[28] derived a more general refractive index expression based on the Mie theory. Their expression for the dispersion refractive index n_{12} as a function of the particle refractive index n_1 reads

$$\frac{dn_{12}}{dc} = \frac{3n_1 \mathrm{Re}(j_1)_{\theta=180°}}{2\alpha^3 \rho_2} \tag{15}$$

where c is the weight concentration in g/cm^3, ρ_2 is the particle density, and $\mathrm{Re}(j_1)_{180°}$ is the real part of the complex amplitude function $(j_1)_{180°}$ which pertains to the light scattering in the forward direction of the primary beam characterized by the angle $\theta = 180°$.[26] The expression for $(j_1)_{180°}$ from the Mie theory[10] is

$$(j_1)_{180°} = \sum_{n=1}^{\infty} \frac{2n+1}{2n(n+1)} (a_n - b_n) \tag{16}$$

with a_n and b_n as mentioned earlier. Equation (15) does not contain the restriction that α be small and allows calculation of the effect of light scattering on the refractive index of a scattering colloidal dispersion. The quantity dn_{12}/dc is essentially constant for values of c below 1×10^{-4} g/cm^3.[29]

Figure 21 shows experimental results obtained for the monodisperse polystyrene standards ranging from 88 to 357 nm in diameter, using a Brice–Phoenix differential refractometer.[5] The wavelength of light used was 546.1 nm, hence the maximum value of α was 2.0. In this range, linear Δn–c behavior is expected[27] and is shown by these data. Measurement scatter is due most likely to adsorbed surfactant and limited instrument resolution (differences measured only to the fifth place). The straight line through the data was calculated using the Lorentz–Lorentz equation from Table II, which is the limiting form of eq. (15) for very small spheres. The favorable comparison between the experimental results and calculated values indicate the reliability of the theory as has been similarly observed by others.[29]

Figure 22 illustrates the effect of wavelength on the refractometer relative signal intensity. A comparison with the turbidimetric counterpart is shown in Figure 23, where nonabsorbing as well as absorbing particles are considered. These calculations illustrate that differential refractometry shows a less dramatic dependence on particle size than turbidimetry of nonadsorbing particles. However, when the particles become absorbing, turbidimetric detection shows a dramatic change to the extent of matching and even improving relative signal dependence on particle size.

Since it is customary in HDC to make injections of samples with nearly the same solid content (0.01%), it is interesting to note comparisons of the relative signal based on the same weight of solids. Figure 24 shows this comparison for turbidimetric detection of absorbing and nonadsorbing particles and for refractometric detection. Although little apparent improvement is offered with turbidimetric detection of absorbing spheres over differential refractometric detection, it must be pointed out that the sensitivity of available differential refractometers is limited to 10^{-7} RIU (refractive index units). Since the solid content of the injected sample is on the order of 0.01 wt-% and further dilution of nearly 20 times occurs by dispersion before the sample enters the signal detection device, the signal intensity will be very weak. This can also be concluded from Figure 24 and points to the need for higher concentrations with the possibility of attendant clogging problems with refractometry.

SUMMARY AND CONCLUSIONS

The results of the calculations presented in this paper can be summarized as follows:

1. The assumption of Gaussian spreading along with a polynomial expansion for the distribution function enabling the application of the Hermite orthogonal polynomials gives inaccurate particle size distributions and inflates the distribution in the direction of smaller-diameter particles. This is a result of the particle scattering cross section–diameter relationship and also the non-Gaussian spreading in the monodisperse standards.
2. An integral method assuming a non-Gaussian spreading function and a polynomial expansion to represent the distribution function (with coefficients determined by a square error criterion) gives PSD values in reasonable agreement with measured values for polydisperse systems of broad distribution. However, for systems with discontinuities in the distribution function, the PSD does not compare favorably.
3. The numerical least-squares method with linear programming showed an oscillation problem similar to that of previous GPC studies which makes the method unreliable for PSD determination.
4. The second method of Ishige et al. eliminates negative values in the distribution function as well as oscillation problems. However, PSD values are still inflated toward small particles.
5. A variation of the second method of Ishige et al. accounting for contributions to the signal of neighboring sizes gives good results for broad and narrow distributions as well as for discontinuous distributions.
6. Theoretical analysis of the different detection methods available suggests that photometric detection at wavelengths where the latexes are light absorbers provides a relative signal comparable to that obtained from a differential refractometer. However, an at least onefold increase in the amount of latex injected, as compared to the amount necessary with a photometer, is needed to provide a good signal in a differential refractometer. These higher concentrations of injected latexes may eventually lead to frequent clogging problems in the HDC columns. Therefore, variable-wavelength photometric detection appears more attractive.

This work is being supported by a grant from the National Science Foundation, Number ENG 77-07041, and by funds from the Emulsion Polymers Institute Industrial Liaison Program.

References

1. H. Small, *J. Coll. Interfac. Sci.*, **48,** 147 (1974).
2. A. J. McHugh, C. A. Silebi, G. W. Poehlein, and J. W. Vanderhoff, *Colloid and Interface Science,* Vol. IV, "Hydrosols and Rheology," 549 (1976).
3. C. A. Silebi and A. J. McHugh, *Emulsions, Latices, and Dispersion,* P. Becher and M. N. Yudenfreund, Eds, Marcel-Dekker, New York, 1978, p. 155.
4. C. A. Silebi and A. J. McHugh, A.I.Ch.E.J., **24,** 204 (1978).
5. C. A. Silebi, Ph.D. Thesis, Lehigh University, June 1978.
6. N. Friis and A. E. Hamielec, *Adv. Chromatogr.*, **13,** 41 (1975).
7. E. A. DiMarzio and C. M. Guttman, *Macromolecules,* **3,** 131 (1970).
8. R. F. Stoisits G. W. Poehlein, and J. W. Vanderhoff, *J. Coll. Interfac. Sci.* **57,** 337 (1976).
9. H. Brenner and L. J. Gaydos, *ibid.*, **58,** 312 (1977).
10. G. Mie, *Ann. Phys.*, **25,** 377 (1908).
11. W. Heller and R. N. Tabibian, *J. Coll. Interfac. Sci.*, **12,** 25 (1957).
12. J. G. Carter, T. M. Jelinek, R. N. Hamm, and R. D. Birkhoff, *J. Chem. Phys.*, **44,** 2266 (1966).
13. R. H. Partridge, *ibid.*, **47,** 4223 (1967).
14. S. W. Churchill, G. C. Clark, and G. C. Sliepscevich, *Disc. Faraday Soc.*, **30,** 192 (1960).
15. W. Heller and W. J. Pargonis, *J. Chem. Phys.*, **26,** 498 (1957).
16. M. Kerker, *The Scattering of Light and Other Electromagnetic Radiation,* Academic Press, New York, 1969.
17. L. H. Tung, *J. Appl. Polym. Sci.*, **10,** 375 (1966).
18. R. F. Stoisits, M.S. Thesis, Lehigh University, 1975.
19. T. Provder and E. M. Rosen, *Separ. Sci.*, **5,** 437 (1970).
20. K. S. Chang and Y. M. Huang, *J. Appl. Polym. Sci.*, **16,** 329 (1972).
21. H. E. Pickett, M. J. R. Cantow, and J. F. Johnson, *J. Appl. Polym. Sci. C,* **21,** 67 (1968).
22. J. Scolere, M.S. Thesis, Lehigh University, 1977.
23. T. Ishige, S. I. Lee, and A. E. Hamielec, *J. Appl. Polym. Sci.*, **15,** 1607 (1971).
24. H. Coll and G. R. Fague, paper presented at Cleveland–Akron GPC/LC Symposium, Cleveland, Ohio, April 1977.
25. A. L. Aden, *J. Appl. Phys.*, **22,** 601 (1951).
26. M. Tryon and E. Horswitz, in *High Polymers,* Vol. XII, G. M. Kline, Ed., Part II, Interscience, New York, 1962.
27. W. Heller, *Phys. Rev.*, **68,** 5 (1945).
28. B. H. Zimm and W. B. Dandliker, *J. Phys. Chem.*, **58,** 644 (1954).
29. M. Nakagaki and W. Heller, *J. Appl. Phys.*, **27,** 975 (1956).

Received February 23, 1978